# POLITECNICO DI TORINO
## Repository ISTITUZIONALE

Successive spike times predicted by a stochastic neuronal model with a variable input signal

(Article begins on next page)

17 May 2024

# SUCCESSIVE SPIKE TIMES PREDICTED BY A STOCHASTIC NEURONAL MODEL WITH A VARIABLE INPUT SIGNAL

GIUSEPPE D'ONOFRIO AND ENRICA PIROZZI

Dipartimento di Matematica e Applicazioni
Università degli studi di Napoli, FEDERICO II, Via Cinthia, Monte S.Angelo
Napoli, 80126, Italy

ABSTRACT. Two different stochastic processes are used to model the evolution of the membrane voltage of a neuron exposed to a time-varying input signal. The first process is an inhomogeneous Ornstein-Uhlenbeck process and its first passage time through a constant threshold is used to model the first spike time after the signal onset. The second process is a Gauss-Markov process identified by a particular mean function dependent on the first passage time of the first process. It is shown that the second process is also of a diffusion type. The probability density function of the maximum between the first passage time of the first and the second process is considered to approximate the distribution of the second spike time. Results obtained by simulations are compared with those following the numerical and asymptotic approximations. A general equation to model successive spike times is given. Finally, examples with specific input signals are provided.

1. **Introduction.** The first passage time (FPT) problem for a stochastic process through a threshold has numerous applications in the studies on neural information coding ([1],[8],[13]). Under a common scenario, the membrane voltage of a neuron fluctuates in response to synaptic input signals and an internal noise. As soon as a threshold voltage is crossed, the neuron fires a spike (action potential). Therefore, the generation of the action potential corresponds to the first passage of the fluctuating membrane voltage through the threshold. Most researchers in the field map the dynamics of a neuronal output to an input signal, internal noise and a specified threshold voltage (see, for instance, [8], [12], [21], [23]). This kind of models often relies on the use of the Ornstein-Uhlenbeck (OU) process ([16],[26]), although sometimes shortcomings have been highlighted (for instance, [20]). Having extensively studied the Gauss-Markov (GM) processes ([2]-[7]), that generalize the OU process, we model the neuronal activity by using this mathematical abstraction.

In neuronal coding studies the interest is mainly focused on the rate codes, i.e. the average number of spikes per unit of time, and on the temporal codes, in which the timing of action potentials is related to the information transmission. The latter codes are of primary interest when the neuron is subject to a time-varying input. Indeed, in the models the voltage after a spike is fixed to a reset value, while the input signal continues without any reset. In this context, some authors

---

are interested in the spike times corresponding to the crossings at particular points of the firing threshold ([21], [22]), while some others study the occurrence of spike trains that adapt to the action of input signals ([12]) or the generation of temporal patterns of spikes in response to fluctuating current injections (frozen noise) ([10], [25]). Stochastic processes different from the OU model are also considered for neuronal modeling, even if results in closed form are known only in few cases (for instance, [17] and references therein). Recently, for a Brownian motion driven by an exponential time-dependent drift in [27] the FPT density was derived as a series expansion of solutions of recurrence equations. Stimulated by these arguments and other interesting results ([8],[11]-[15], [18], [20]-[24]), our aim is to show how the GM processes theory can provide approximations of the firing distributions and, in particular, to contribute to the modeling of successive spike times. Here, we focus our attention on the second spike time and we model it by means of the FPT of a new GM process. This process is constructed *ad hoc* for embodying the memory of a spike already occurred while taking into account the ongoing action of the input signal.

Starting from a Leaky Integrate-and-Fire (LIF) equation ([1]) with a time-varying input signal, we model the first spike time by using the related FPT random variable through a constant threshold; then, we define another GM process to describe the behavior of the membrane voltage after the first spike. For this specific process, we derive the corresponding stochastic differential equation (SDE) and investigate its FPT. In order to have two (ordered) successive times, we consider the maximum between the two FPTs and we use the probability density function (PDF) of this maximum to approximate the PDF of the second spike time. For the general successive spike times the results can be accordingly generalized.

2. **The model.** In order to describe the occurrence of firing times $T_0, T_1, \ldots, T_n$ of a neuron subject to an input signal, we consider the FPT $\mathcal{T}_k$ of a stochastic process $V_k(t)$ (for $k = 1, \ldots, n$) through a constant threshold $S$. We model the behavior of the neuronal membrane potential by diffusion processes $\{V_1(t), V_2(t), \ldots, V_n(t)\}$ such that $\{V_k(t), t \geq t_0\}$ (for $k = 1, \ldots, n$) is solution of the SDE

$$dV_k = \left\{ -\alpha V_k + \alpha \left[ V_{rest} + \frac{I(t)}{\alpha} \right] \mathbb{P}(T_{k-1} \leq t) \right\} dt + \sigma dW, \quad V_k(t_0) = v_0 < S, \quad (1)$$

with $t_0 \geq 0$, $\mathbb{P}(T_0 = t_0) = 1$. In (1) the parameter $1/\alpha (> 0)$ is the characteristic (decay) time of the membrane potential, $V_{rest}$ is the resting potential, $v_0$ is the initial value, $\sigma(> 0)$ represents a constant intensity of the noise and $W$ the standard Brownian motion. Furthermore, $I(t)$ stands for a time-dependent input signal never reset. It can be generated by an injected input current or a synaptic current originated from the surrounding neuronal activity. Here, the $\mathbb{P}(T_{k-1} \leq t)$ is the probability that the previous spike time $T_{k-1}$ has already occurred, with reference to time $t$. Therefore, we provide evaluations of $\mathbb{P}(T_k \leq t)$ (for $k \geq 1$) by using an approach based on theoretical and numerical results about the FPT $\mathcal{T}_k$ of the processes $V_k(t)$.

For comparison we consider a LIF model with reset which is described by equation (1) without index $k$, with $\mathbb{P}(T_{k-1} \leq t) = 1$. Assuming $T_0 = t_0$, let $T_1$ be the FPT through the firing threshold $S$ of the solution process $V(t)$ ($= V_1(t)$ for $t_0 \leq t \leq T_1$) with reset to $v_0$, i.e. $V(T_1^+) = v_0$. $T_1$ stands for the first spike (firing) time. Following the time evolution of the process $V(t)$ for $t \geq T_1$, the second passage time $T_2$ occurs and it stands for the second spike time, and so on. It is possible to

obtain random samples $T_0, T_1, \ldots, T_n$ of successive spike times simulating random paths of $V(t)$ by applying the well-known Euler discretization method to its SDE and recording the crossing times of $S$.

By using our previous results ([2]-[7]), we are able to specify $V_1(t)$ and to obtain approximations for the PDF of its FPT $\mathcal{T}_1$, such that $\mathbb{P}(T_1 \leq t) = \mathbb{P}(\mathcal{T}_1 \leq t)$. In Section 3 we introduce the process $V_2(t)$ and its FPT $\mathcal{T}_2$ useful to model the second spike time $T_2$. Finally, assuming $\Theta_1 = \mathcal{T}_1$, we consider $\Theta_2 = \max\{\Theta_1, \mathcal{T}_2\}$ and thus

$$\mathbb{P}(T_2 \leq t) \approx \mathbb{P}(\Theta_2 \leq t).$$

For the $k$-th spike time, the following approximation can be given: $\mathbb{P}(T_k \leq t) \approx \mathbb{P}(\Theta_k \leq t)$ where $\Theta_k = \max\{\Theta_{k-1}, \mathcal{T}_k\}$. In Section 4 we give an exponential approximation valid for the PDF of the first spike and show how it can help for evaluating the PDF of the second spike. In Section 5 some examples of applications are given.

2.1. **Modeling the first spike time.** Let us start by considering the process $V_1(t)$ solution of SDE (1) for $k = 1$ with $\mathbb{P}(T_0 = t_0) = 1$. According to [2], under hypotheses of regularity on the function $I(t)$, and due to the form of its infinitesimal moments: $A_1^{(1)}(v, t) = -\alpha (v - V_{rest}) + I(t)$, $A_2^{(1)}(t) \equiv \sigma^2$, the diffusion process $V_1(t)$ is a Gauss-Diffusion (GD) process. It is also a GM process, i.e. a Gaussian process identified by the mean and by a special covariance (see, for details, [9]). Denoting, for $\tau \leq t$,

$$\mathcal{M}_1(t|\tau) = V_{rest} \left(1 - e^{-\alpha(t-\tau)}\right) + e^{-\alpha t} \int_\tau^t I(\xi) e^{\alpha\xi} d\xi, \tag{2}$$

it is characterized by the mean and covariance functions

$$m_{V_1}(t|v_0, t_0) \quad = v_0 e^{-\alpha(t-t_0)} + \mathcal{M}_1(t|t_0), \tag{3}$$

$$c_{V_1}(s, t|t_0) \quad = \frac{\sigma^2}{2\alpha} e^{-\alpha(t-t_0)} \left[e^{\alpha(s-t_0)} - e^{-\alpha(s-t_0)}\right] \qquad (t_0 \leq s \leq t) \tag{4}$$

with the following transition PDF, for $\tau \leq t$,

$$f_{V_1}[x, t|y, \tau] = \frac{\sqrt{\alpha}}{\sqrt{\pi\sigma^2(1 - e^{-2\alpha(t-\tau)})}} \exp\left\{-\alpha \frac{\left[x - y e^{-\alpha(t-\tau)} - \mathcal{M}_1(t|\tau)\right]^2}{\sigma^2 \left(1 - e^{-2\alpha(t-\tau)}\right)}\right\}. \tag{5}$$

Note that the above PDF is a normal-type transition function with the conditional mean $\mathbb{E}[V_1(t)|V_1(\tau) = y] = m_{V_1}(t|y, \tau)$, and the variance $Var(t|\tau) = c_{V_1}(t, t|\tau)$.

The FPT $\mathcal{T}_1$ of the process $V_1(t)$ through a constant threshold S is defined as:

$$\mathcal{T}_1 := \inf_{t \geq t_0} \{t : V_1(t) \geq S\} \quad \text{with} \quad V_1(t_0) = v_0 < S$$

and with the PDF $g_1(S, t|v_0, t_0)$. For input signals $I(t)$ such that the integral $\int_{t_0}^t I(\xi) e^{\alpha\xi} d\xi$ exists for any $t \geq t_0$, we are able to provide a numerical approximation of the PDF $g_1(S, t|v_0, t_0)$ solving, by a numerical procedure ([2],[9]), the following non singular second kind Volterra integral equation ([9]):

$$g_1(S, t|v_0, t_0) = -\Psi_1[S, t|v_0, t_0] + \int_{t_0}^t \Psi_1[S, t|S, \tau] g_1(S, \tau|v_0, t_0) d\tau \tag{6}$$

with

$$\Psi_1[S, t|y, \tau] = f_{V_1}[S, t|y, \tau]$$
$$\times \left\{-\frac{S\alpha(1 + e^{-2\alpha(t-\tau)})}{1 - e^{-2\alpha(t-\tau)}} + \frac{2\alpha y e^{-\alpha(t-\tau)}}{1 - e^{-2\alpha(t-\tau)}} - [\alpha V_{rest} + I(t)] + \frac{2\alpha \mathcal{M}_1(t|\tau)}{1 - e^{-2\alpha(t-\tau)}}\right\}. \tag{7}$$
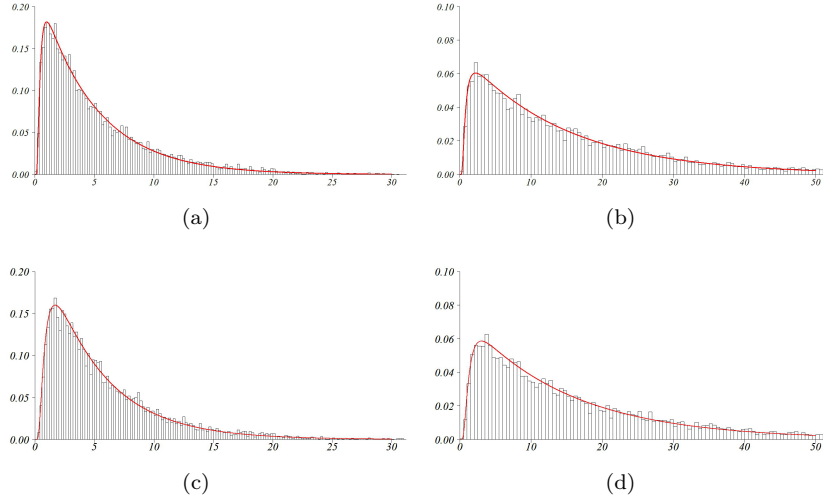
FIGURE 1. Histograms of $10^4$ FPTs $\mathcal{T}_1$ of simulated random paths of $V_1(t)$ by discretization of (1) for $k = 1$ and numerical $\widehat{g}_1(t)$ for $S = 1.5$ (1(a),1(c)) and $S = 2$ (1(b),1(d)). $I(t) \equiv \mu = 0.25$, $\alpha = 1$, $V_{rest} = 0.2$, $\sigma = 1$, $t_0 = 0$,$v_0 = 0$ in 1(a),1(b) and $v_0 = -0.5$ in 1(c),1(d). The discretization step for simulations and for the numerical procedure is $10^{-3}$.

We underline that we can provide evaluations of $g_1(S, t|v_0, t_0)$ by means of a numerical quadrature ([2]) specialized for the case of time-varying input signal $I(t)$. Then, also $\mathbb{P}(\mathcal{T}_1 \leq t)$ can be evaluated. In Fig. 1 we compare our numerical approximation $\widehat{g}_1(t)$ of $g_1(S, t|v_0, t_0)$ with the histograms of simulated FPTs for different threshold values and starting points $v_0$. The firing density is represented by histograms of a sample of FPTs $\mathcal{T}_1$ (or $T_1$), through a constant threshold, of simulated random paths obtained from equation (1) for $k = 1$, discretized by means of the Euler method.

Now, we can proceed considering a new SDE, i.e. the SDE (1) for $k = 2$ in order to model the successive spike time.

3. **Modeling the second spike time.** We now focus our attention on another stochastic process by which we describe the evolution of the neuronal membrane potential in the presence of the threshold $S$ *before the spike time* $T_2$. We consider a process $V_2(t)$, linked to the process $V_1(t)$, starting from the reset value $v_0$ with covariance (4) and the following mean function

$$m_{V_2}(t|v_0, t_0) = v_0 e^{-\alpha(t-t_0)} + \mathcal{M}_2(t|t_0) \tag{8}$$

where we define

$$\mathcal{M}_2(t|t_0) = \mathbb{E}\left\{\mathbb{E}\left[\mathcal{M}_1(t|t_1)|T_1 = t_1\right]\right\} = \int_{t_0}^{t} \mathcal{M}_1(t|t_1)g_1(S, t_1|v_0, t_0)dt_1. \tag{9}$$

**Remark 1.** The formula (9) takes into account the probability that each time instant $t_1$ before $t$ could have been an instant of first spike (i.e. a realization of $T_1$). This specific mathematical condition is motivated by the assumption that the

average behavior of the neuronal membrane after a spike time (and reset) is almost the same of the ones before the spike, although in any time $t$ it *has to remind* the occurrence of a previous spike and *has to continue* to be subject to the input signal which in the meanwhile has never been reset. With these reasons in mind, we construct the *ad hoc* process $V_2(t)$ as a transformed $V_1(t)$ by (9). Moreover, as will be clear in the next proposition, the (9) leads to set a SDE of type (1) that, from the mathematical point of view, can be properly handled.

**Proposition 1.** *The process $V_2(t)$, obtained from the process $V_1(t)$ by (9), having mean defined by (8) and covariance as in (4), is a GM process and is solution of the following SDE, for $t \geq t_0$,*

$$dV_2 = \left\{ -\alpha V_2 + \alpha \left[ V_{rest} + \frac{I(t)}{\alpha} \right] \mathbb{P}(T_1 \leq t) \right\} dt + \sigma dW, \quad V_2(t_0) = v_0. \qquad (10)$$

*Proof.* From (2), (8) and (9), the mean function (8) of $V_2(t)$ becomes

$$m_{V_2}(t|v_0, t_0) = v_0 e^{-\alpha(t-t_0)} + e^{-\alpha t} \left[ \alpha V_{rest} \int_{t_0}^{t} \mathbb{P}(T_1 \leq \xi) e^{\alpha \xi} d\xi + \int_{t_0}^{t} I(\xi) \mathbb{P}(T_1 \leq \xi) e^{\alpha \xi} d\xi \right]. \qquad (11)$$

Due to the linearity of relations (8) and (9), or equivalently from (11), and due to the form of covariance (4), the process $V_2(t)$ is a GM process. Moreover, we note that the specified process $V_2(t)$ is characterized by the normal transition PDF

$$f_{V_2}[x, t|y, \tau] = \frac{\sqrt{\alpha}}{\sqrt{\pi \sigma^2 (1 - e^{-2\alpha(t-\tau)})}} \exp \left\{ -\alpha \frac{\left[ x - y e^{-\alpha(t-\tau)} - \mathcal{M}_2(t|\tau) \right]^2}{\sigma^2 \left( 1 - e^{-2\alpha(t-\tau)} \right)} \right\}, \quad (12)$$

having the same variance of $V_1(t)$ and the following conditional mean

$$\mathbb{E}[V_2(t)|V_2(\tau) = y] = y e^{-\alpha(t-\tau)} + \mathcal{M}_2(t|\tau) \qquad (13)$$

where

$$\mathcal{M}_2(t|\tau) = e^{-\alpha t} \left[ \alpha V_{rest} \int_{\tau}^{t} \mathbb{P}(T_1 \leq \xi) e^{\alpha \xi} d\xi + \int_{\tau}^{t} I(\xi) \mathbb{P}(T_1 \leq \xi) e^{\alpha \xi} d\xi \right], \qquad (14)$$

and, in particular, from (11),

$$\mathcal{M}_2(t|\tau) = m_{V_2}(t|v_0, t_0) - e^{-\alpha(t-\tau)} m_{V_2}(\tau|v_0, t_0). \qquad (15)$$

Finally, by using the differentiable mean function (11), recalling (14) and (15), along the lines of [9], the infinitesimal drift of $V_2(t)$ is evaluable in the following way

$$\begin{aligned} A_1^{(2)}(v, t) &= \lim_{\Delta t \to 0} \frac{\mathbb{E}[V_2(t + \Delta t) - V_2(t)|V_2(t) = v]}{\Delta t} \\ &= m'_{V_2}(t|v_0, t_0) - \alpha [v - m_{V_2}(t|v_0, t_0)] = \mathcal{M}'_2(t|\tau) - \alpha [v - \mathcal{M}_2(t|\tau)] \\ &= -\alpha v + \alpha \left[ V_{rest} + \frac{I(t)}{\alpha} \right] \mathbb{P}(T_1 \leq t). \end{aligned}$$

The infinitesimal variance is also evaluable and we have $A_2^{(2)}(t) \equiv \sigma^2$. Hence, under hypotheses of regularity on the functions involved in the infinitesimal drift, $V_2(t)$ is also a diffusion process (i.e. GD) and solves the SDE (10).                    □

Similarly to the previous section, we now consider the FPT for $V_2(t)$, i.e.

$$\mathcal{T}_2 := \inf_{t \geq t_0} \{ t : V_2(t) \geq S \} \quad \text{with} \quad V_2(t_0) = v_0 < S. \qquad (16)$$

Let $g_2(S, t|v_0, t_0)$ be the PDF of $\mathcal{T}_2$, i.e. $g_2(S, t|v_0, t_0) = \dfrac{d\mathbb{P}(\mathcal{T}_2 \leq t)}{dt}$. It is solution of

$$g_2(S, t|v_0, t_0) = -\Psi_2[S, t|v_0, t_0] + \int_{t_0}^{t} \Psi_2[S, t|S, \tau] g_2(S, \tau|v_0, t_0) d\tau \qquad (17)$$

with

$$\Psi_2[S, t|y, \tau] = f_{V_2}[S, t|y, \tau]$$
$$\times \left\{ -\frac{S\alpha(1+e^{-2\alpha(t-\tau)})}{1 - e^{-2\alpha(t-\tau)}} + \frac{2\alpha y e^{-\alpha(t-\tau)}}{1 - e^{-2\alpha(t-\tau)}} - [\alpha V_{rest} + I(t)]\,\mathbb{P}(T_1 \leq t) + \frac{2\alpha \mathcal{M}_2(t|\tau)}{1 - e^{-2\alpha(t-\tau)}} \right\} \qquad (18)$$

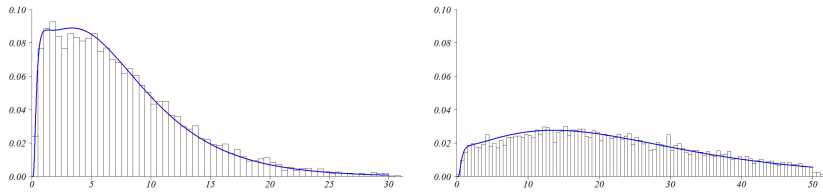where $f_{V_2}[S, t|y, \tau]$ and $\mathcal{M}_2(t|\tau)$ are as in (12) and (14), respectively.



FIGURE 2. Histograms of $10^4$ simulated $\mathcal{T}_2$ and numerical $\widehat{g}_2(t)$ for $S = 1.5$ (on the left) and $S = 2$ (on the right). $I(t) \equiv \mu = 0.25$, $\alpha = 1$, $V_{rest} = 0.2$, $v_0 = 0$, $\sigma = 1$. The discretization step for the simulation is $10^{-3}$ and for the numerical procedure is $10^{-2}$.

We provide numerical estimations $\widehat{g}_2(t)$ of $g_2(S, t|v_0, t_0)$ by solving numerically (17) and compare them with simulation results of (10). We remark that in this case our numerical procedure to solve (17), that involves the function (18), requires to evaluate in advance $g_1(S, t|v_0, t_0)$ as solution of (6) and then $\mathbb{P}(T_1 \leq t)$. Hence, an iterative numerical strategy has been adequately carried out to evaluate finally $\widehat{g}_2(t)$. Similarly, the simulation algorithm applied to (10) is based on the previous evaluation of $\mathbb{P}(T_1 \leq t)$ as described in Section 2.1. In Fig. 2 the satisfactory agreement between simulations of $V_2(t)$ by discretization of (10) and our numerical approximations $\widehat{g}_2(t)$ highlights the accuracy of our numerical results.

3.1. **Comparing the FPT densities.** For a constant input $I(t) \equiv \mu$, see Fig. 3 for comparisons between the behaviors of $\widehat{g}_1(t)$ and $\widehat{g}_2(t)$. The evident difference between the curves of $\widehat{g}_1(t)$ and $\widehat{g}_2(t)$ in Fig. 3 motivated the following proposition.
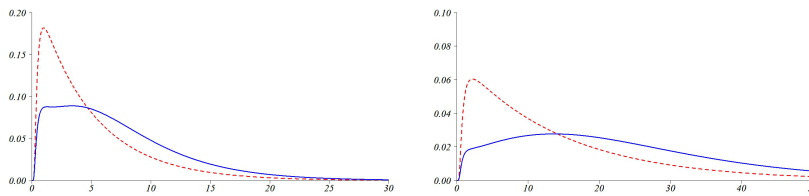


FIGURE 3. On the left: $\widehat{g}_1(t)$ (red dashed) and $\widehat{g}_2(t)$ (blue solid) for $S = 1.5$; the other parameters are as in Fig. 1(a) and as in the left side of Fig. 2. On the right: the same for $S = 2$; the other parameters are as in Fig. 1(b) and as in the right side of Fig. 2 .

It is useful for the following Proposition to recall from [19] that the random variable $X$ is *smaller* than the random variable $Y$ in the usual *stochastic order* (denoted by $X \leq_{st} Y$) if and only if

$$\mathbb{P}(X \geq u) \leq \mathbb{P}(Y \geq u) \quad \forall u \in (-\infty, \infty).$$

**Proposition 2.** *The FPT $\mathcal{T}_1$ of $V_1(t)$ and the FPT $\mathcal{T}_2$ of $V_2(t)$ are stochastically ordered as follows*

$$\mathcal{T}_1 \leq_{st} \mathcal{T}_2.$$

*Proof.* We note that on the basis of (9), from (14), recalling (2),

$$\mathcal{M}_2(t|\tau) \leq \mathcal{M}_1(t|\tau)\mathbb{P}(T_1 \leq t), \quad \forall t > \tau \geq t_0 \tag{19}$$

and from (8) and (2), we have

$$m_{V_2}(t|v_0, t_0) \leq m_{V_1}(t|v_0, t_0), \quad \forall t \geq t_0, \, v_0 < S. \tag{20}$$

(See Fig. 4 for the case of a constant input signal $I(t) \equiv \mu$.) Recalling that $V_1(t)$ and $V_2(t)$ are GM processes, it is known ([2],[9]) that both are transformed process by the Brownian motion $W(\cdot)$ as follows

$$V_j(t) = m_{V_j}(t|v_0, t_0) + \sigma e^{-\alpha(t-t_0)} W\left(\frac{e^{2\alpha(t-t_0)} - 1}{\alpha}\right), \forall t \geq t_0, \text{ for } j = 1, 2. \tag{21}$$

Hence, taking into account (20) and (21), we can write

$$\mathbb{P}(\mathcal{T}_1 \leq t) = \mathbb{P}\left(\max_{t_0 \leq \tau \leq t} V_1(\tau) \geq S\right) \geq \mathbb{P}\left(\max_{t_0 \leq \tau \leq t} V_2(\tau) \geq S\right) = \mathbb{P}(\mathcal{T}_2 \leq t), \quad \forall t \geq t_0.$$

Hence,

$$\mathbb{P}(\mathcal{T}_1 \geq t) \leq \mathbb{P}(\mathcal{T}_2 \geq t), \quad \forall t \geq t_0$$

i.e. $\mathcal{T}_1 \leq_{st} \mathcal{T}_2$. □

Again from [19], if $\mathcal{T}_1 \leq_{st} \mathcal{T}_2$ then $\mathbb{E}(\mathcal{T}_1) \leq \mathbb{E}(\mathcal{T}_2)$.
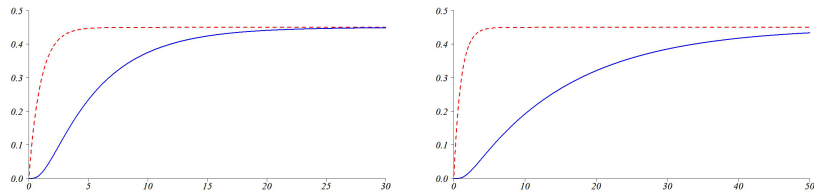


FIGURE 4. Plots of the $m_{V_1}(t|v_0, t_0)$ (red dashed) and $m_{V_2}(t|v_0, t_0)$ (blue solid) for $S = 1.5$ (on the left) and $S = 2$ (on the right). The other parameters are as in Fig. 3.

3.2. **Ordering the FPTs.** Since $\mathbb{P}(\mathcal{T}_2 < \mathcal{T}_1) \geq 0$, we assume $\Theta_1 = \mathcal{T}_1$ and consider the random variable $\Theta_2 = \max\{\Theta_1, \mathcal{T}_2\}$ for which $\mathbb{P}(\Theta_2 < \mathcal{T}_1) = 0$, being $\mathbb{P}(\Theta_2 \geq \mathcal{T}_1) = 1$ from its definition, with PDF

$$g_{\Theta_2}(t) = g_1(t)\mathbb{P}(\mathcal{T}_2 \leq t) + g_2(t)\mathbb{P}(\mathcal{T}_1 \leq t) \tag{22}$$

where for shortness $g_1(t) = g_1(S, t|v_0, t_0)$ and $g_2(t) = g_2(S, t|v_0, t_0)$.

Following our numerical strategy, evaluations of the functions involved in (22) are available, and finally also the evaluation of $\mathbb{P}(\Theta_2 \leq t)$ can be given by means of a quadrature applied to $g_{\Theta_2}(s)$ for $t_0 \leq s \leq t$.

The random variable $\Theta_2$ turns out to be a more suitable tool for modeling the second spike time. Indeed, in all cases of applications, and how it will be shown for specified examples in the following, the numerical evaluation of (22) fits the histogram of the simulated $T_2$ better than the $\widehat{g}_2(t)$ (see Fig.8), where $T_2$ is the second passage time of $V(t)$ through the threshold S.

We also provide a scatter plot to give some indications about the joint distribution of the pairs of the two spike times (see Fig. 5).
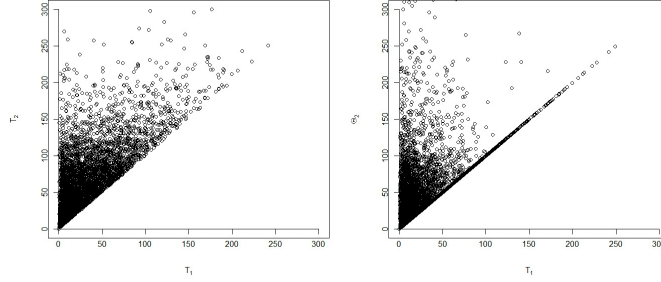


FIGURE 5. Scatter plots of $5 \cdot 10^3$ pairs $(T_1, T_2)$ on the left, and of $(T_1, \Theta_2)$ on the right. $(T_1, T_2)$ are simulated first and second passage times of $V(t)$. $(T_1, \Theta_2)$ are pairs with simulated FPT $\mathcal{T}_1 (= T_1)$ of $V_1(t)$ and simulated $\Theta_2 = \max\{\mathcal{T}_1, \mathcal{T}_2\}$, with simulated FPTs $\mathcal{T}_2$ of $V_2(t)$. All parameters are specified in the caption of Fig. 8.

Furthermore, the satisfactory agreement between the numerical evaluation of (22) and the histogram of the maximum of simulated FPTs $\mathcal{T}_1$ and $\mathcal{T}_2$ will be shown. For examples specified in Section 5 these features are highlighted in Fig.7 and Fig.8.

4. **An asymptotic approximation.** At first, we specify an asymptotic approximation valid for the PDF $g_1(S, t|v_0, t_0)$. For asymptotically constant input signals such that $I = \lim\limits_{t \to +\infty} I(t)$ from (2), (3) and (4) we have

$$\lim_{t \to \infty} m_{V_1}(t|v_0, t_0) = V_{rest} + \frac{I}{\alpha}, \quad \lim_{t \to \infty} Var(t|\tau) = \lim_{t \to \infty} \frac{\sigma^2}{2\alpha}\left(1 - e^{-2\alpha(t-\tau)}\right) = \frac{\sigma^2}{2\alpha}.$$

Hence, we obtain the stationary transition density function $\mathcal{W}_1(x)$, i.e

$$\mathcal{W}_1(x) = \lim_{t \to \infty} f_{V_1}[x, t|y, \tau] = \sqrt{\frac{\alpha}{\pi\sigma^2}} \exp\left\{-\frac{\alpha}{\sigma^2}\left[x - \left(V_{rest} + \frac{I}{\alpha}\right)\right]^2\right\}. \tag{23}$$

From (7) and (23), we also obtain that

$$h_{V_1} = -\lim_{t \to \infty} \Psi_1(S, t|y, \tau) = \left\{ \alpha \left[ S - \left( V_{rest} + \frac{I}{\alpha} \right) \right] \right\} \mathcal{W}_1(S) =$$

$$= \alpha \sqrt{\frac{\alpha}{\pi \sigma^2}} \left[ S - \left( V_{rest} + \frac{I}{\alpha} \right) \right] \exp \left\{ -\frac{\alpha}{\sigma^2} \left[ S - \left( V_{rest} + \frac{I}{\alpha} \right) \right]^2 \right\}. \quad (24)$$

Along the lines of [2], for $t - t_0 > 1/\alpha$ and $S - \left( V_{rest} + \dfrac{\max\limits_{t_0 \leq t} I(t)}{\alpha} \right) > \sqrt{\sigma^2 \alpha}$, then

the following exponential approximation for $g_1(S, t|v_0, t_0)$ holds:

$$g_1[S, t|v_0, t_0] \approx \widetilde{g}_1(t) = h_{V_1} e^{-h_{V_1}(t-t_0)}. \quad (25)$$

Using the approximation $\widetilde{g}_1(t)$ as in (25), we can also write that, $\forall t \geq t_0$,

$$\mathbb{P}(T_1 \leq t) \approx \widetilde{\mathbb{P}}(\mathcal{T}_1 \leq t) = 1 - e^{-h_{V_1}(t-t_0)}. \quad (26)$$

Then, we adopt the closed form expression of $\widetilde{\mathbb{P}}(\mathcal{T}_1 \leq t)$ in (11) in place of $\mathbb{P}(T_1 \leq t)$ and we finally obtain

$$\widetilde{m}_{V_2}(t|v_0, t_0) = v_0 e^{-\alpha(t-t_0)} + \widetilde{\mathcal{M}}_2(t|t_0) \quad (27)$$

with

$$\begin{aligned} \widetilde{\mathcal{M}}_2(t|t_0) &= V_{rest} \left( 1 - e^{-\alpha(t-t_0)} \right) \left[ 1 + \frac{\alpha e^{-h_{V_1}(t-t_0)}}{h_{V_1} - \alpha} \right] \\ &+ e^{-\alpha t} \int_{t_0}^t I(\xi) e^{\alpha \xi} d\xi - e^{-\alpha t} \int_{t_0}^t I(\xi) e^{-(h_{V_1}-\alpha)(\xi-t_0)} d\xi. \end{aligned} \quad (28)$$

We point out that now we have the closed form expressions $\widetilde{\mathbb{P}}(\mathcal{T}_1 \leq t)$ and $\widetilde{\mathcal{M}}_2(t|\tau)$ useful in place of $\mathbb{P}(T_1 \leq t)$ and $\mathcal{M}_2(t|\tau)$ in (10) and (18), respectively. An immediate benefit is that we can again exploit all the results of Section 3: indeed, our numerical quadrature to solve (17), and the simulation strategy of (10), for evaluating the PDF $g_2(S, t|v_0, t_0)$, can be now directly applied without any previous numerical evaluations of $g_1(S, t|v_0, t_0)$ and $\mathbb{P}(T_1 \leq t)$, but using the closed form expressions $\widetilde{g}_1(t)$ and $\widetilde{\mathbb{P}}(\mathcal{T}_1 \leq t)$ of (25) and (26), respectively.

Furthermore, for $\Theta_2$ we proceed as follows. Let $\widehat{g}_2[t; \widetilde{g}_1(t)]$ ($\widehat{\mathbb{P}}[\mathcal{T}_2 \leq t; \widetilde{g}_1(t)]$) be the numerical evaluation of $g_2(t)$ ($\mathbb{P}(\mathcal{T}_2 \leq t)$) obtained by using the asymptotic expression $\widetilde{g}_1(t)$ of $g_1(t)$, we give the following approximation $\gamma_{\Theta_2}(t)$ for $g_{\Theta_2}(t)$:

$$\gamma_{\Theta_2}(t) = h_{V_1} e^{-h_{V_1}(t-t_0)} \widehat{\mathbb{P}}[\mathcal{T}_2 \leq t; \widetilde{g}_1(t)] + \widehat{g}_2[t; \widetilde{g}_1(t)] \left( 1 - e^{-h_{V_1}(t-t_0)} \right). \quad (29)$$

At the end of the next section, we will give an example in which the asymptotic approximations can be used.

## 5. Examples of application: Exponential and constant input signals. We consider the following exponential form to represent an input signal:

$$I(t) = \mu + \lambda e^{-\beta t} \quad \text{with } \beta > 0, \mu, \lambda \in \mathbb{R}, \quad t \geq t_0 = 0. \quad (30)$$

Now, the SDE for $V_1(t)$ is the following one:

$$dV_1 = [-\alpha(V_1 - V_{rest}) + \mu + \lambda e^{-\beta t}]dt + \sigma dW, \quad V_1(t_0) = v_0 \quad t \geq t_0. \quad (31)$$

In this case, we find

$$\mathcal{M}_1(t|\tau) = \left(V_{rest} + \frac{\mu}{\alpha}\right)\left(1 - e^{-\alpha(t-\tau)}\right) + \frac{\lambda}{\alpha - \beta}\left(e^{-\beta t} - e^{-\alpha(t-\tau)-\beta\tau}\right) \quad (32)$$

by which we are able to specify the mean, the covariance, the conditional moments and the transition PDF of the process $V_1(t)$ as in Section 2.1. In particular, for evaluating $g_1(S,t|v_0,t_0)$, in the corresponding integral equation we can specify $\Psi_1[S,t|y,\tau]$ as in (7) with $I(t)$ as in (30) and $\mathcal{M}_1(t|\tau)$ as in (32). Furthermore, from (9), we can specify the process $V_2(t)$ with

$$\mathcal{M}_2(t|\tau) = e^{-\alpha t}\left[(\alpha V_{rest} + \mu)\int_\tau^t \mathbb{P}(T_1 \leq \xi)e^{\alpha\xi}d\xi + \lambda\int_\tau^t e^{(\alpha-\beta)\xi}\mathbb{P}(T_1 \leq \xi)d\xi\right]. \quad (33)$$

From Proposition 1, the mean, the covariance, the conditional moments, the transition PDF of the process $V_2(t)$ are available and $V_2(t)$, for the input signal (30), satisfies the following SDE:

$$dV_2 = \left[-\alpha V_2 + \alpha\left(V_{rest} + \frac{\mu + \lambda e^{-\beta t}}{\alpha}\right)\mathbb{P}(T_1 \leq t)\right]dt + \sigma dW, \quad V_2(t_0) = v_0,\ t \geq t_0. \quad (34)$$

Finally, for evaluating $g_2(S,t|v_0,t_0)$, from (17) we can specify $\Psi_2[S,t|y,\tau]$ of (18) with $I(t)$ as in (30), $\mathcal{M}_2(t|\tau)$ as in (33) and $\mathbb{P}(T_1 \leq t)$ as the numerical evaluation $\widehat{\mathbb{P}}(\mathcal{T}_1 \leq t)$, having already obtained $\widehat{g}_1(t)$ for $g_1(S,t|v_0,t_0)$. See in Fig. 6 (left) the comparison between histograms of $\mathcal{T}_1$ by simulations of (31) and numerical approximations $\widehat{g}_1(t)$. See in Fig. 6 (right) the comparison between histograms of $\mathcal{T}_2$ by simulations of (34) and numerical approximations $\widehat{g}_2(t)$.
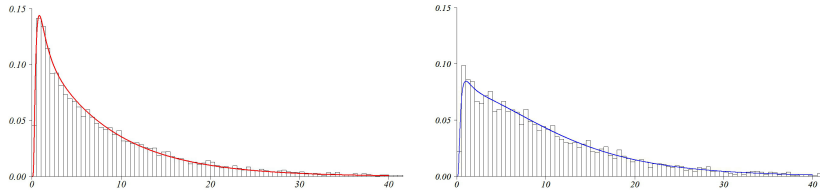


FIGURE 6. Left: histograms of $10^4$ simulated $\mathcal{T}_1$ and numerical $\widehat{g}_1(t)$. Right: histograms of $10^4$ simulated $\mathcal{T}_2$ and numerical $\widehat{g}_2(t)$ for exponential input signal with $\lambda = 0.25$, $\beta = 1.5(> \alpha)$, $\mu = 0$, $\alpha = 1$, $V_{rest} = 0.2$, $v_0 = 0$, $\sigma = 1$ and $S = 1.5$. The discretization step for the simulation is $10^{-3}$ and for the numerical procedure is $10^{-3}$ on the left and is $10^{-2}$ on the right.

To validate the accuracy of numerical approximations of $g_{\Theta_2}(t)$, on the left of figures 7-8 we show the satisfactory agreement between the numerical evaluation of $g_{\Theta_2}(t)$ (22) and the histogram of the maximum of simulated FPTs $\mathcal{T}_1$ and $\mathcal{T}_2$. On the right of figures 7-8 we provide a comparison between the numerical evaluation of $g_{\Theta_2}(t)$ (22) and the histogram of simulated $T_2$, i.e. the second passage time of $V(t)$ through the threshold S. Specifically, $T_2$ is obtained by simulating the SDE of $V(t)$ for $t \geq T_1$ with $V(T_1^+) = v_0$; the first time $t(\geq T_1)$ such that $V(t) \geq S$ is recorded as the simulated value of $T_2$. In particular, on the right of Fig. 8 also $\widehat{g}_2(t)$ is plotted. Note that while Fig. 7 refers to the case $\beta > \alpha$, Fig. 8 refers to the case $\beta < \alpha$; in particular, the case $\beta < \alpha$ corresponds to the case in which the time-varying effect of the input signal persists beyond the time of decay to the
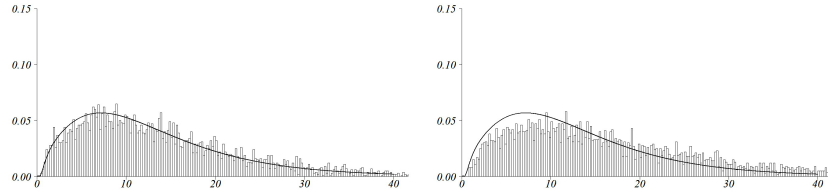
FIGURE 7. Left: histograms of the simulated $\Theta_2 = \max\{\mathcal{T}_1, \mathcal{T}_2\}$ and the numerical evaluation of $g_{\Theta_2}(t)$ (22) for an exponential input signal. Right: histograms of $10^4$ simulated $T_2$ and the numerical evaluation of $g_{\Theta_2}(t)$. The values of parameters are the same of Fig. 6. The discretization step for the numerical procedure is $10^{-2}$ and for simulations is $10^{-2}$ on the left and $10^{-4}$ on the right.
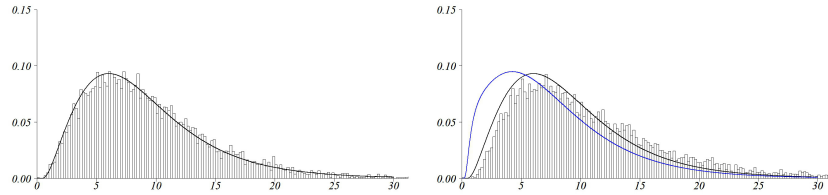


FIGURE 8. Left: histograms of the simulated $\Theta_2 = \max\{\mathcal{T}_1, \mathcal{T}_2\}$ and the numerical evaluation of $g_{\Theta_2}(t)$ (22) for an exponential input signal are shown. Right: histograms of $10^4$ simulated $T_2$, the numerical evaluation of $g_{\Theta_2}(t)$ (in black) and $\widehat{g}_2(t)$ (in blue). The values of parameters are: $\lambda = 0.2$, $\beta = 0.01 (< \alpha)$, $\mu = 0.1$, $\alpha = 1$, $V_{rest} = 0.2$, $v_0 = -0.5$, $\sigma = 1$ and $S = 1.5$. The discretization steps are as in Fig. 7.

resting level of the potential, whereas the case $\beta > \alpha$ corresponds to the case in which the time-varying effect of the signal is short and vanishes before than the potential attains the resting level.

Alternatively, it also possible to use the approximation $\widetilde{\mathbb{P}}(\mathcal{T}_1 \leq t)$ for $\mathbb{P}(T_1 \leq t)$ as in (26). Indeed, following the lines of Section 4, in this case from (30) and (32) we have

$$I \equiv \lim_{t \to +\infty} I(t) = \mu, \quad \lim_{t \to \infty} \mathcal{M}_1(t|y, \tau) = V_{rest} + \frac{\mu}{\alpha}, \tag{35}$$

and, from (23),

$$\mathcal{W}_1(x) = \sqrt{\frac{\alpha}{\pi \sigma^2}} \exp\left\{ -\frac{\alpha}{\sigma^2} \left[ x - \left( V_{rest} + \frac{\mu}{\alpha} \right) \right]^2 \right\}. \tag{36}$$

Therefore, for $t - t_0 > 1/\alpha$ and $S - \left( V_{rest} + \frac{\mu+\lambda}{\alpha} \right) > \sqrt{\sigma^2 \alpha}$ the asymptotic approximation (26) is valid with $h_{V_1}$ as in (24) with $\mu$ in place of $I$. Finally, it is possible to use for the process $V_2(t)$ the approximated mean function $\widetilde{m}_{V_2}(t|v_0, t_0)$ from (27), evaluated with the signal $I(t)$ as in (30).

From our simulations and numerical evaluations, we can see that it is possible to exploit the asymptotic approximation $\widetilde{\mathbb{P}}(\mathcal{T}_1 \leq t)$ for threshold $S = 2$ and the values of other parameters as in Fig. 1 (for the constant signal) and in Fig. 6 (for

the exponential signal). An example of application is considered for values of the parameters specified as in the caption of Fig. 9. In this case, it is possible to evaluate $\widehat{g}_2[t; \widetilde{g}_1(t)]$, by using the asymptotic $\widetilde{g}_1(t)$, and finally $\gamma_{\Theta_2}(t)$ as in (29).
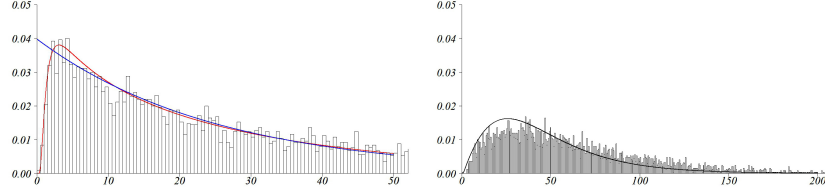


FIGURE 9. Left: histograms of $10^4$ simulated $\mathcal{T}_1$, compared to the numerical $\widehat{g}_1(t)$ (in red) and the asymptotic approximation $\widetilde{g}_1(t)$ (in blue) for an exponential input signal with $\lambda = 0.1$, $\beta = 0.1 (< \alpha)$, $\mu = 0.1$, $\alpha = 1$, $V_{rest} = 0.1$, $v_0 = -0.5$, $\sigma = 1$ and $S = 2$. Right: histograms of $10^4$ simulated $T_2$ and the numerical evaluation of $\gamma_{\Theta_2}(t)$ (29) for the same choice of parameters. The discretization step for the numerical procedure is $10^{-3}$, for simulations is $10^{-4}$.

Finally, we give some indications about a quantitative error analysis: the $\mathcal{L}^1$-norm of the difference between two interpolating densities of histograms from two independent samples of $T_2$ is about 0.08, while the $\mathcal{L}^1$-norm of the difference between one of these densities and the numerical evaluation of $g_{\Theta_2}(t)$ is about 0.54 for the case of Fig. 7. The $\mathcal{L}^1$-norm of the difference related to independent histograms of $T_2$ is about 0.12 for the case of Fig. 8 (0.1 for Fig. 9), while the $\mathcal{L}^1$-norm of the difference between the histogram of $T_2$ and the numerical $g_{\Theta_2}(t)$ is about 1.2 for Fig. 8 (1.02 for Fig. 9).

6. **Conclusion.** The present paper introduces a new model which extends our theoretical approach for particular GM processes and their applications in neuronal modeling, in particular for the case of the first and the second spike time. In summary, the main innovative point is the introduction of the model for the second spike generation by which we provide approximations for the PDF of the second spike time. Our results aim to contribute to the theory of the temporal (or timing) codes. They can be extended to the case of special input signals, for instance, to those of [21].

## REFERENCES

[1] A. N. Burkitt, A review of the integrate-and-fire neuron model: I. Homogeneous synaptic input, *Biological Cybernetics*, **95** (2006), 1–19.

[2] A. Buonocore, L. Caputo, E. Pirozzi and L. M. Ricciardi, The first passage time problem for Gauss-diffusion processes: Algorithmic approaches and applications to LIF neuronal model, *Methodol. Comput. Appl. Prob.*, **13** (2011), 29–57.

[3] A. Buonocore, L. Caputo, E. Pirozzi and L. M. Ricciardi, On a stochastic leaky integrate-and-fire neuronal model, *Neural Computation*, **22** (2010), 2558–2585.

[4] A. Buonocore, L. Caputo, E. Pirozzi and M. F. Carfora, Gauss-diffusion processes for modeling the dynamics of a couple of interacting neurons, *Math. Biosci. Eng.*, **11** (2014), 189–201.

[5] A. Buonocore, L. Caputo, A. G. Nobile and E. Pirozzi, Gauss–Markov processes in the presence of a reflecting boundary and applications in neuronal models, *Applied Mathematics and Computation*, **232** (2014), 799–809.

[6] A. Buonocore, L. Caputo, A. G. Nobile and E. Pirozzi, Restricted Ornstein–Uhlenbeck process and applications in neuronal models with periodic input signals, *Journal of Computational and Applied Mathematics*, **285** (2015), 59–71.

[7] A. Buonocore, L. Caputo, A. G. Nobile and E. Pirozzi, Gauss-markov processes for neuronal models including reversal potentials, *Advances in Cognitive Neurodynamics (IV)*, **11** (2015), 299–305.

[8] M. J. Chacron, K. Pakdaman and A. Longtin, Interspike interval correlations, memory, adaptation, and refractoriness in a leaky integrate-and-fire neuron with threshold fatigue. *Neural Computation*, **15** (2003), 253–276.

[9] E. Di Nardo, A. G. Nobile, E. Pirozzi and L. M. Ricciardi, A computational approach to first passage-time problems for Gauss-Markov processes, *Adv. Appl. Prob.*, **33** (2001), 453–482.

[10] J. M. Fellous, P. H. Tiesinga, P. J. Thomas and T. J. Sejnowski, Discovering spike patterns in neuronal responses, *The Journal of Neuroscience*, **24** (2004), 2989–3001.

[11] V. Giorno and S. Spina, On the return process with refractoriness for a non-homogeneous Ornstein-Uhlenbeck neuronal model, *Math. Bios. Eng.*, **11** (2014), 285–302.

[12] H. Kim and S. Shinomoto, Estimating nonstationary inputs from a single spike train based on a neuron model with adaptation, *Math. Bios. Eng.*, **11** (2014), 49–62.

[13] P. Lánský and S. Ditlevsen, A review of the methods for signal estimation in stochastic diffusion leaky integrate-and-fire neuronal models, *Biol. Cybern.*, **99** (2008), 253–262.

[14] P. Lánský, Sources of periodical force in noisy integrate-and-fire models of neuronal dynamics, *Physical Review E*, **55** (1997), 2040–2043.

[15] B. Lindner, Interspike interval statistics for neurons driven by colored noise, *Physical Review E*, **69** (2004), 022901–1–022901–4.

[16] L. M. Ricciardi and L. Sacerdote, The Ornstein-Uhlenbeck process as a model for neuronal activity, *Biological Cybernetics*, **35** (1979), 1–9.

[17] L. M. Ricciardi, A. Di Crescenzo, V. Giorno and A. G. Nobile, An outline of theoretical and algorithmic approaches to first passage time problems with applications to biological modeling, *Mathematica Japonica*, **50** (1999), 247–322.

[18] T. Schwalger, F. Droste and B. Lindner, Statistical structure of neural spiking under non-Poissonian or other non-white stimulation, *Journal of Computational Neuroscience*, **39** (2015), 29–51.

[19] M. Shaked and J. G. Shanthikumar, *Stochastic Orders and Their Applications*, Academic Press, Boston (USA), 1994.

[20] S. Shinomoto, Y. Sakai and S. Funahashi, The Ornstein-Uhlenbeck process does not reproduce spiking statistics of cortical neurons, *Neural Computation*, **11** (1997), 935–951.

[21] T. Taillefumier and M. 0. Magnasco, A phase transition in the first passage of a Brownian process through a fluctuating boundary: Implications for neural coding, *PNAS,* **110** (2013), E1438–E1443.

[22] T. Taillefumier and M. Magnasco, A transition to sharp timing in stochastic leaky integrate-and-fire neurons driven by frozen noisy input, *Neural Computation*, **26** (2014), 819–859.

[23] T. Taillefumier and M. Magnasco, A fast algorithm for the first-passage times of Gauss-Markov processes with Holder continuous boundaries, *J. Stat. Phys.*, **140** (2010), 1130–1156.

[24] P. J. Thomas, A lower bound for the first passage time density of the suprathreshold Ornstein-Uhlenbeck process, *J. Appl. Probab.*, **48** (2011), 420–434.

[25] J. V. Toups, J. M. Fellous, P. J. Thomas, T. J. Sejnowski and P. H. Tiesinga, Multiple spike time patterns occur at bifurcation points of membrane potential dynamics, *PLoS Comput. Biol.*, **8** (2012), e1002615, 1–19.

[26] H. C. Tuckwell, *Stochastic Processes in the Neurosciences*, SIAM, 1989.

[27] E. Urdapilleta, Series solution to the first-passage-time problem of a Brownian motion with an exponential time-dependent drift, *J. Stat. Phys.,* **140** (2010), 1130–1156.

*E-mail address*: giuseppe.donofrio@unina.it
*E-mail address*: enrica.pirozzi@unina.it